Solid State Electronics 164 (2020) 107743

Contents lists available at ScienceDirect

Solid State Electronics

journal homepage: www.elsevier.com/locate/sse

# Delineation of point defect state in Czochralski Si by modified background haze

Anselmo Jaehyeong Lee*, Don-Ha Hwang, Hee-Bog Kang, Bo-Young Lee

*R&D Center, SK Siltron, 39387, Suchul-daero 435, Gumi-si, Gyeongsangbuk-do, South Korea*

ARTICLE INFO

The review of this paper was arranged by "Jung-Hee Lee"

*Keywords:*
Point defect
Czochralski Si
Cone defect
Background haze
Oxidation

ABSTRACT

A novel haze technique for analyzing point-defect distribution in Czochralski Si (CZ-Si) wafers without intentional contamination by transition metals was proposed. Based on the background haze in high-temperature oxidation, a three-step oxidation process including two-step low-temperature precipitation and a single-step high-temperature wet oxidation process was designed. After the newly designed heat processing and preferential etching, surface haze was formed selectively on the interstitial-dominant region of the wafer. Through electron microscopy analysis, surface defects decorated with Ni were observed, which suggested that the surface accumulation of non-gettered Ni adsorbed from the furnace causes surface haze on the interstitial-dominated region. The widths of the hazes could be optimized by adjusting the processing times of the first two steps, which affected the Ni gettering ability in the vacancy-dominated regions of the wafers. Additionally, the second stage at 1000 °C was associated with precipitate growth, as well as with haze formation.

## 1. Introduction

In conventional Czochralski Si (CZ-Si), oxygen precipitates (OPs) are among the most important defects formed in substrates for semiconductor device processing [1,2]. For example, OPs contribute to enhanced device yields by providing intrinsic gettering sites for metal contaminants in the active area of the Si substrate [3–5]; they also induce leakage current failure in various device structures [6,7] and form cone defects in shallow-trench isolation (STI) structures after reactive ion etching (RIE) [8,9]. Moreover, with excessive precipitation, the mechanical strength of the wafer degrades, yielding wafer deformation [10]. In addition, OPs become sources of extended defects like oxidation-induced stacking faults (OISF) under elevated-temperature oxidation when the residual vacancy (V) supersaturation in the as-grown Si crystal is significantly high [11–13]. Thus, gathering detailed information on the distribution of precipitated oxygen and the residual point defect state is important for controlling defects in CZ-Si wafers; this data should be provided before designing Si wafers with the desired properties for advanced semiconductor devices.

OPs can be directly measured by laser-scattering tomography (LST) or optical microscopy combined with preferential etching of heat-treated wafers. In addition, measuring the residual vacancy concentration is possible via deep-level transient spectroscopy (DLTS) in Pt-diffused Si wafers [14]. Also, the concentration of vacancy–oxygen complexes, which act as seeds for oxygen precipitation, were recently measured by low-temperature Fourier-transform infrared (FTIR) spectroscopy in rapid thermal processed (RTP) wafers [15,16]. However, these techniques are commonly low-throughput and require complicated and time-consuming wafer pre-treatment. Therefore, faster and easier methods to evaluate OPs or point defect distributions should be introduced for the mass production of high-purity Si wafers.

The haze phenomenon, or the formation of metal silicide etch pits on the surface of contaminated Si wafers after heat processing and preferential etching [17], is considered a fast method for visualizing the distribution of point defect regions in Si wafers [18,19]. In this method, the difference in the gettering ability of the oxygen precipitation distribution of wafers is a major property that endows selectivity to metal haze formation. To do this, a method for achieving homogeneous contamination of a metal element in the wafer surface at a desired surface concentration should be achieved as a prior technology. Typically, Cu [18–20] and Ni [21] are used in the haze method because of their fast diffusion and high solid solubility in crystalline Si [22,23]. However, strong acids such as hydrofluoric acid (HF), hydrochloric acid (HCl), and nitric acid ($HNO_3$) combined with a dedicated wet etch system should be prepared to perform the haze test. In addition, using transition metals can provide contamination sources that are

* Corresponding author.
*E-mail addresses:* jaehyeong.lee1@sk.com (A.J. Lee), donha.hwang1@sk.com (D.-H. Hwang), heebog.kang@sk.com (H.-B. Kang), boyoung.lee1@sk.com (B.-Y. Lee).

https://doi.org/10.1016/j.sse.2019.107743

Available online 02 December 2019

detrimental to wafer production. Therefore, it is necessary to develop a new haze technique with performance equivalent to that of typical contamination-based haze methods but free from the issues on the cost, safety and process contamination.

Shimura et al. reported the formation of small saucer pits with areal densities of $> 1.0 \times 10^6$ cm$^{-2}$ on Si wafer surfaces after oxidation in a "not clean" furnace at temperatures > 1100 °C [24–26]. The saucer pit generation was attributed to stacking faults on the wafer surfaces induced by transition metal contamination from the furnace; this mechanism was confirmed by transmission electron microscope (TEM) analysis. Stacy et al. reported "background haze" on clean Si wafers after wet oxidation at 1150 °C [27], similar to the results in Ref. [24]. They also identified the background contaminants as Cu by analyzing haze-related defects with energy-dispersive X-ray spectroscopy (EDS) and selective diffraction patterns. They indicated that contamination sources could be introduced to generate haze-related defects in Si wafers during high-temperature oxidation processes. In Si wafer processing, the development of haze without intentional contamination is desirable; however, no studies have yet investigated the optimization of this phenomenon for analyzing the point defect states in Si wafers.

In this study, we proposed a new procedure for selective formation of the background haze on the interstitial-dominated region of the Si wafer surface and compared it to the typical Cu haze and other methods. We also evaluated the results of the new haze test and discussed the underlying features of this method in more detail.

## 2. Experimental

### 2.1. Sample preparation and defect characterization

For these experiments, p-type, 200-mm, (1 0 0) oriented 725-μm-thick polished Si wafers prepared from lightly B-doped CZ-Si crystals were used. The B doping concentration estimated from the resistivity (1–10 Ω·cm) of the wafers as obtained by the four-point probe method was $0.13–1.45 \times 10^{16}$ cm$^{-3}$, and the initial oxygen concentration ([$O_i$]) was $4.9–5.2 \times 10^{17}$ cm$^{-3}$ with the conversion factor of $3.14 \times 10^{17}$ cm$^{-3}$ recommended in the ASTM F1188 standard for room-temperature FTIR spectroscopy. Samples were chosen from the four different pulling rate conditions in a CZ-Si ingot to obtain various point defect states, ranging from vacancy-dominated to interstitial-dominated in nature [13,28].

Firstly, the point defect states of samples from each position were evaluated by the Cu haze process described in Ref. [20], with the surface Cu concentration of $> 1.0 \times 10^{15}$ cm$^{-2}$ and subsequent annealing in $N_2$ ambient at temperatures of < 1100 °C to diffuse Cu into the Si bulk. Then, the samples were preferentially etched in Wright etchant [29] for 5 min followed by cleaning in deionized water (DIW) and inspected under a halogen lamp to verify the surface haze distributions. Simultaneously, Cu haze widths were measured from the wafer center with the precision of 0.5 mm. Boundary of the two point defect regions was considered as the position where the haze defects were completely disappeared. Due to the rough boundary shape of the Cu haze, uncertainty of the measurement was estimated as ± 5 mm.

Other samples were used for simulating cone defect formation [8,9] after annealing at 780 °C for 3 h followed by 1000 °C for 16 h in a conventional vertical furnace with $N_2$ ambient. After that, samples were dry-etched in an 8-inch RIE chamber using $Cl_2$ + HBr + $O_2$ plasma with a target selectivity of $SiO_2$:Si = 1:100. Then, cone defect distributions were measured by surface LST with a resolution of ≥17 nm and a penetration depth of ~1 μm. The impurity concentration and point defect state analyzed for each sample group are summarized in Table 1.

### 2.2. Design of a new haze procedure and evaluation

Based on the background haze phenomenon, a three-step oxidation process combining a low-temperature two-step precipitation and a high-temperature single-step wet oxidation was designed. During the precipitation step, samples were treated at 870 °C and then 1000 °C to form slightly grown OPs [30,31] to getter ambient metal contaminants in the vacancy-dominated region. The effect of each step on the final haze state was verified by changing the annealing conditions. Firstly, the annealing time was changed from 90 to 480 min for the first step and from 60 to 420 min for the second step, respectively. Each step was performed in dry $O_2$ ambient to enhance metal-induced microdefect formation at the wafer surface. After annealing, samples were subjected to wet oxidation in 1150 °C for 100 min with mixed $H_2$ and $O_2$ gas to generate large-sized haze-related defects. The ramp-up and -down rates of the furnace were set to 5 °C/min and 3 °C/min, respectively; the final oxide thickness was ~10,000 Å as measured by Elli-SE spectroscopic ellipsometry (SE) equipment of Ellipso Technology. A schematic of the multi-step oxidation process performed is shown in Fig. 1.

Before etching, the coordinates of defects in the haze region of wafers were obtained by surface LST. Afterward, the microstructures of several source defects in the haze region were analyzed by TEM, followed by sampling with a focused ion beam (FIB) instrument. In the meantime, other heat-treated samples were dipped in 30 vol% of diluted hydrofluoric acid (DHF) for 5 min to remove the thick oxide layer, which could hinder the following etch process. Next, the samples were dipped in Wright etchant for 5 min to reveal surface haze. Simultaneously, changes in the morphology of the etch pits during preferential etching were confirmed by scanning electron microscopy (SEM). Then, the etched samples were inspected visually and observed by optical microscopy (OM) to verify the distribution of saucer pits in the hazed region. After that, the haze distributions were compared to the results in the Cu haze and RIE process, as confirmed in the previous section.

**Table 1**
Crystal Properties of Samples.

| Group | Pulling rate (Relative) | Point defect state | [$O_i$] ($\times 10^{17}$ cm$^{-3}$) | Cone Defect Density (cm$^{-2}$) |
|---|---|---|---|---|
| A | Very high | Vacancy | 5.07–5.16 | 741.09–13.12 |
| B | High | Vacancy | 5.16–5.21 | 9.79–15.47 |
| C | Low | Interstitial | 5.15–5.21 | 0.21–120.02 |
| D | Very low | Interstitial | 4.94–5.13 | 1.67–5.31 |

Cone defect densities were measured in the 0 and 90 mm from the wafer center, and denoted in the table with same order.

## 3. Results and discussion

### 3.1. Description of the new haze method

Photographs of the etched samples observed after the Cu haze and the new haze heat treatment are presented in Fig. 2(a) and (b). Bright

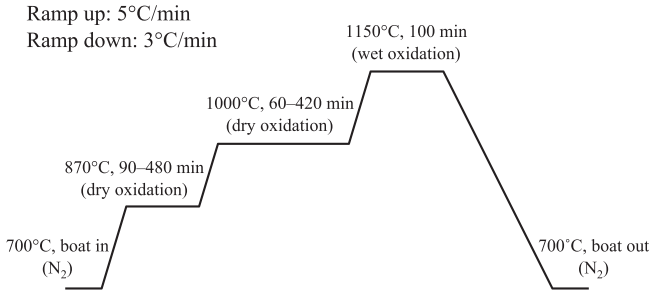


**Fig. 1.** Schematic temperature profile of the multi-step oxidation process used in this study.

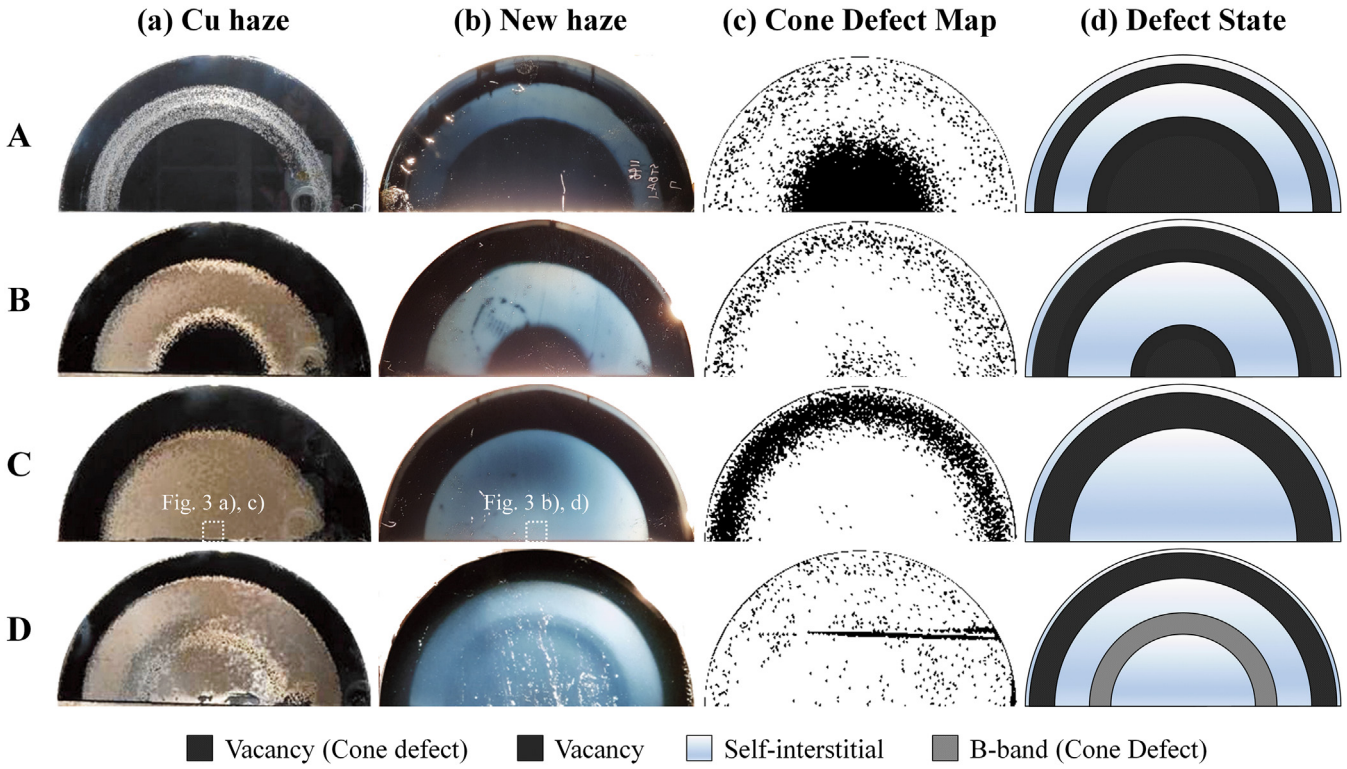


**Fig. 2.** Photographs of COP-free CZ-Si wafers processed after (a) Cu haze and (b) new haze process, taken under spotlight. Locations analyzed by the microscope in group C samples are also shown in the figure. (c) Surface LST defect map of each sample after cone defect simulation process. (d) Schematic diagrams of defect state in each group analyzed by haze test and cone defect simulation.

haze with a bluish-white color is obtained through the new process, whereas a relatively dull yellowish haze appears in the Cu-contaminated wafers. In addition, the cone defect regions presented in Fig. 2(c) and delineated in the RIE process are matched to black-colored regions of the wafers where the contamination species were completely gettered during heat treatment. Also, it was shown that the vacancy region figured in the haze methods is slightly wider than the cone defect region, which represents the gradient of the point defect concentration inside the region. Very sharp boundaries are revealed between the vacancy- and interstitial-dominated regions in the wafer after the new haze process, whereas relatively rough boundaries are formed in the Cu haze process. This indicates that the lower-temperature steps in the new haze process successfully promote selective haze formation to visualize the point defect states in the crystal-originated particle (COP)-free CZ-Si. Another interesting point is that B-band, where the nucleation sites of OPs are provided by supersaturated self-interstitials [32], was detected in a sample of group D that was grown at the lowest pulling rate. Because the B-band has a possibility to form cone defects after the heat process, as shown in Fig. 2(c), it is important to verify that the new haze method can detect the B-band as well as the vacancy region. From the haze test results of group D, it was confirmed that these requirements were met in new haze method.

Fig. 3 shows the morphology of the etch pits in each method as observed by OM and SEM. The microscopy confirms that etch pits in the Cu haze are formed with the density of $\sim 5.0 \times 10^5$ cm$^{-2}$ in cross or asterisk shapes suggesting the dendritic growth of surface Cu during heat treatment because of the high surface contamination level. Meanwhile, the etch pits in the new haze method are revealed as typical saucer pits with a formation density of $> 1.0 \times 10^6$ cm$^{-2}$, similar to the reported value in Ref. [25]. However, the etch pit density changes within the same group depending on the process run; therefore, the etch pit density variation with heat treatment conditions cannot be determined clearly. The etch pits found in the new haze are relatively smaller than in the Cu haze; therefore, they are more clearly observed

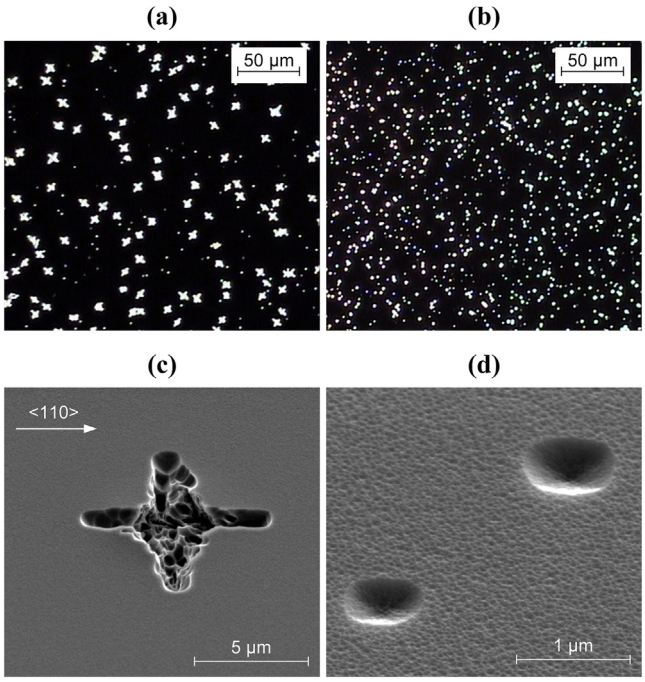


**Fig. 3.** Dark-field optical micrographs of etch pits in a sample of group C delineated by Wright etching for 5 min in (a) Cu haze and (b) new haze, respectively. Tilted SEM images of individual etch pits in (c) Cu haze and (d) new haze specimens are also presented.

in dark-field microscopy. No evidence appears of coarsening in the etch pits of the new haze, indicating that the metal contamination level during the haze process is much lower than the surface Cu concentration used in the Cu haze procedure [20]. Thus, it can be estimated that

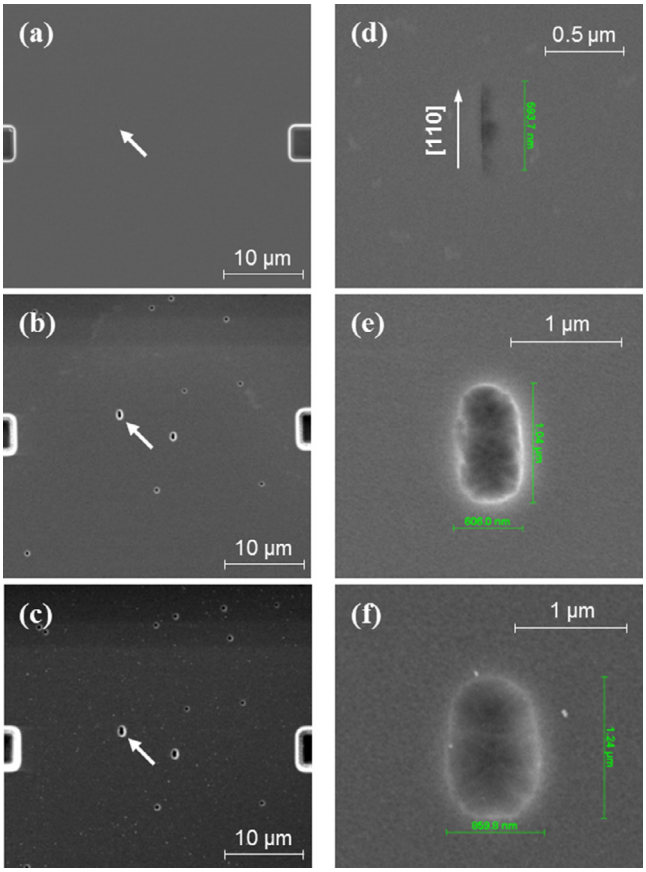


**Fig. 4.** SEM micrographs of haze distribution in a sample of group C observed after (a) DHF etch, (b) DHF + Wright etch for 30 s, and (c) HF + Wright etch for 60 s, respectively. Evolution of the surface defect (denoted by an arrow) into an individual etch pit in the same etch processes is also shown in (d)–(f).

the "resolution" to the boundaries of the point defect region delineated by the diluted-contamination haze in the furnace is much lower than that with the conventional method with the high contamination level, because of the differences in the average sizes of the etch pits.

### 3.2. Characterization of surface defects in haze area

Fig. 4 shows an SEM analysis of the evolution of surface etch pits formed in the haze region in the early stage of the etch step. Beneath the oxide layer, thin traces of 500–700-nm defects are found and identified as possible source defects for new haze. These defect traces are extended into micrometer-scale saucer pits in the Wright etchant in less than 60 s. Interestingly, the buried defects that are not observed after DHF treatment are unveiled after 30 s etching. However, no further addition of etch pits is observed in prolonging the Wright etching step to 60 s, although the individual etch pits are expanded in size, as shown in Fig. 4(c). Based on one-half of the known etch rate (~500 nm/min) given in Ref. [29] and the etch time of 30 s, it could be estimated that most haze-related defects are within ~250 nm of the surface in the interstitial-dominated region where contaminant segregation occurs.

Fig. 5 shows the TEM morphology of a surface microdefect found in the interstitial-dominated region of a sample from group C subjected to the new haze process. As shown in the bright-field image of Fig. 5(a), the surface defect is an extrinsic stacking fault with a length of ~500 nm extended along the ⟨1 1 0⟩ direction. No punched-out dislocations or lattice irregularity are observed around the defect, except in the defective region located in the center of the stacking fault. The high-angle annular dark-field scanning TEM (HAADF-STEM) analysis, presented in Fig. 5(b), shows that several dendritic-shaped defect

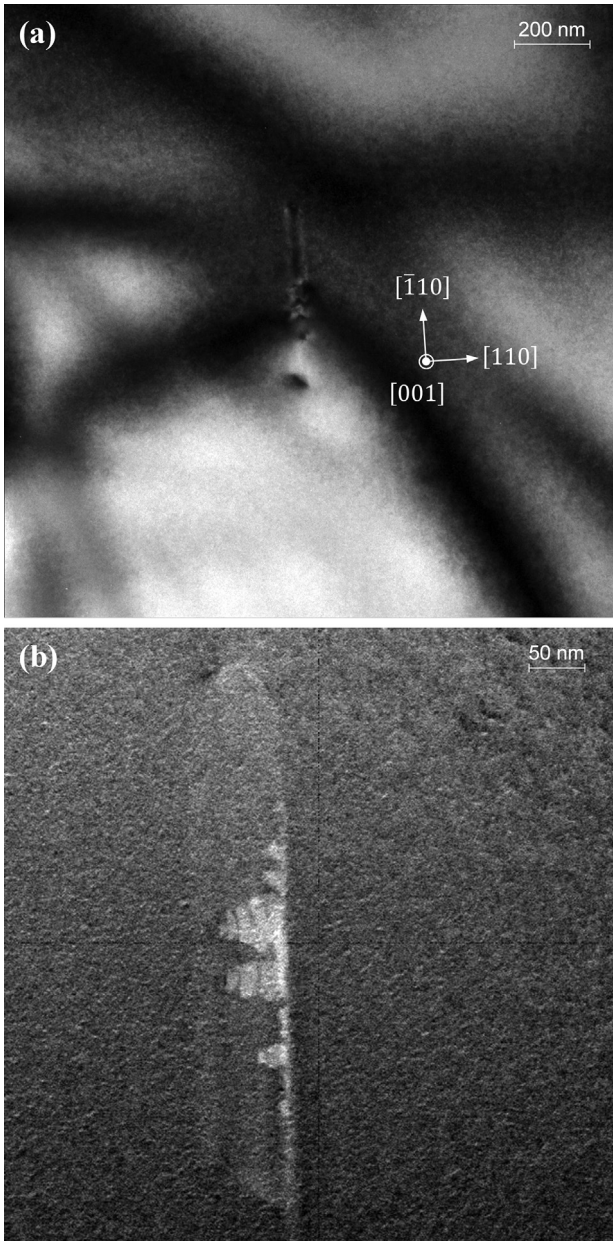


**Fig. 5.** (a) A bright-field, (1 0 0) plane-view TEM micrograph of a stacking fault-type defect in haze region. (b) A HAADF-STEM micrograph of the defect shown in (a), indicating decoration by white-colored metal precipitates.

clusters decorate the stacking fault. As shown in Fig. 6, impurities contained in the dendrites are identified as Ni by a STEM-EDS analysis with the concentration of ~1.4 at%. In addition, a Cu trace exists in both the cluster and the Si matrix, but this is from the Cu grid used in the fabrication of the TEM specimen and is not relevant to defect formation. Other transition metals such as Fe, Co, and Pd, which could induce surface haze [33], are not observed in the clusters. However, no differences appear in the fast Fourier-transform (FFT) pattern of high-resolution TEM images of Ni clusters and the Si (1 0 0) lattice presented in Fig. 7, implying that the lattice of Ni cluster is $NiSi_2$ formed at high temperature, which is difficult to distinguish through FFT analysis. Through direct analysis of the surface defect, it becomes clear that the incorporation of Ni in the high-temperature step is sufficient to achieve Ni supersaturation at the wafer surface during the subsequent cooling period, which is reflected in the Ni precipitate decorating the surface defect.

Besides the heat process, crystal pulling process is a distinctive

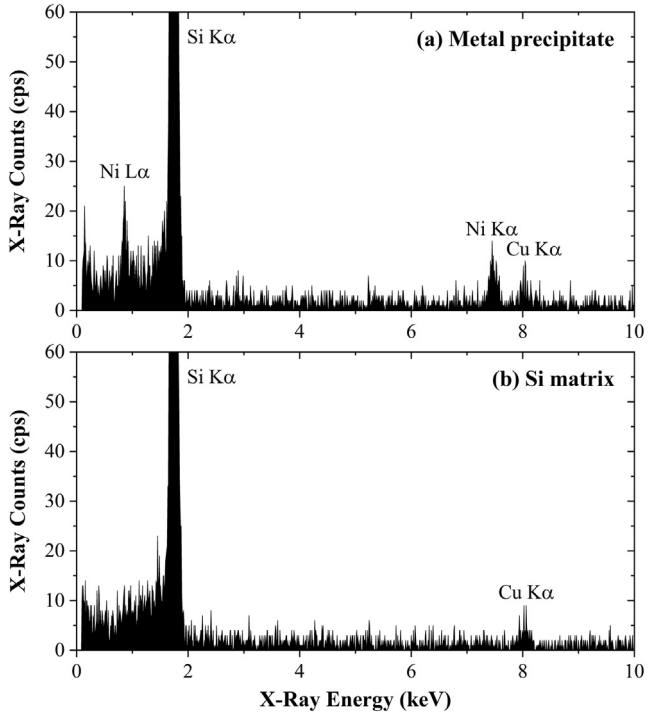


**Fig. 6.** EDS spectra measured in (a) metal precipitate and (b) Si matrix, respectively.

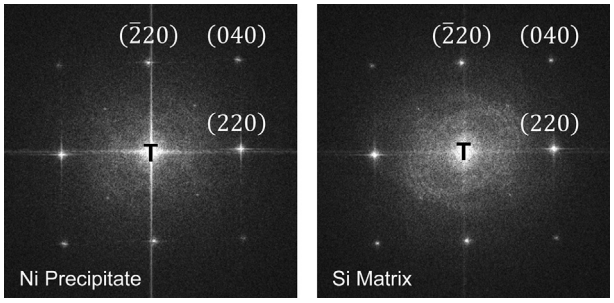


**Fig. 7.** FFT patterns extracted from the high-resolution TEM images of Fig. 5(a) in the metal precipitate (left) and Si matrix (right), respectively.

source of Ni contamination. It was reported that surface segregation of Ni can occur strongly by the bulk Ni introduced from the Si melt, which causes surface defects with high density [34]. However, bulk Ni is easily purified during a CZ process due to its very low equilibrium solid solubility ($k_{eff} \sim 3 \times 10^{-5}$) [35]. Environment of the crystal pulling process is also a clear route of Ni contamination of the ingot surface, but it is expected that Ni introduced in this route would be removed completely after the ingot surface grinding process whose removal thickness is equal to few millimeters. Therefore, the concentration of bulk Ni introduced in the contemporary single crystal pulling process is expected to be negligible compared to the concentration of surface Ni segregated during the wafer heat process.

### 3.3. Process optimization and evaluation

Fig. 8 shows the dependence of haze widths on the annealing times (X, Y) of the first two steps in the proposed haze cycle. The surface contamination level originating from the furnace is non-uniform with the furnace environment and thermal budget. Moreover, the haze intensity observed under spotlight is continuously affected by the etchant conditions and incident light characteristics. Thus, it is practical to measure the haze widths in the interstitial-dominated region instead of

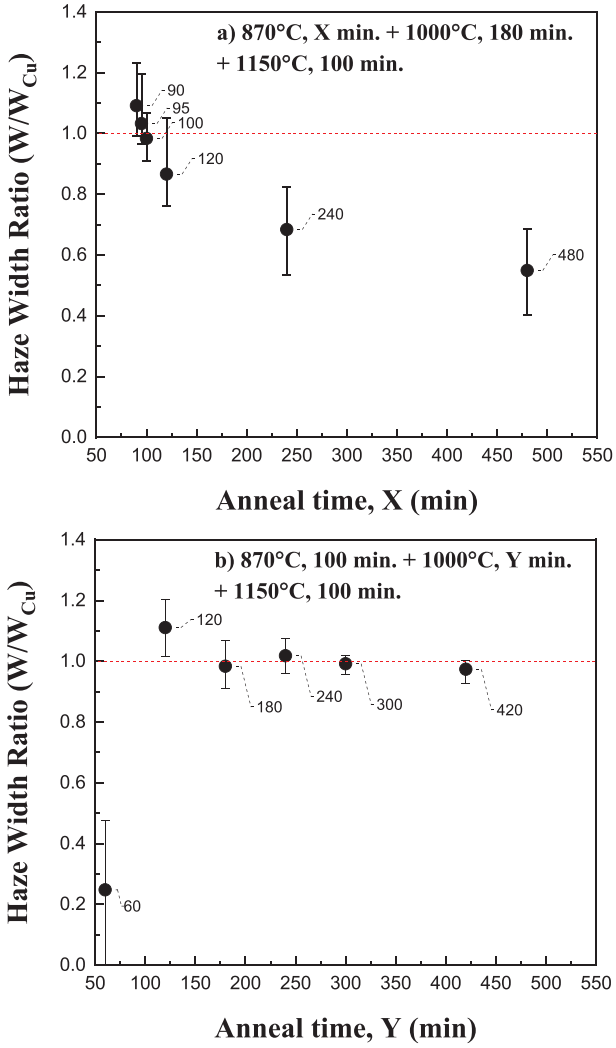


**Fig. 8.** Dependence of haze width ratio ($W/W_{Cu}$) measured in the samples of group B on the (a) first step and (b) second step annealing times, respectively.

the other measurable parameters to describe the haze formation behavior relative to the input conditions. Therefore, $W/W_{Cu}$, i.e., the ratio of the new haze widths (W) to the conventional Cu haze widths ($W_{Cu}$) of each wafer, is measured for the different annealing times. As shown in Fig. 8(a), $W/W_{Cu}$ is inversely proportional with the first-step annealing time X; $W/W_{Cu}$ approaches 1 at X = 100 min. Meanwhile, as shown in Fig. 8(b), the effect of the second-step duration time Y on the haze widths is more complicated. Firstly, the haze itself forms only when Y ≥ 120 min for a fixed X; for Y < 120 min, the haze is non-uniformly formed or even disappeared in some cases. This is represented by $W/W_{Cu}$ values that are relatively low or zero. In addition, the reliable haze formation yielding a result equivalent to the Cu haze method only occurs when Y ≥ 180 min; for shorter durations, the entire wafer surface is covered with haze and $W/W_{Cu}$ is much greater than unity.

Like the other surface haze phenomena, new haze is indirectly figure out the self-interstitial region by suppressing the surface haze at the vacancy region with the differences in the gettering ability. Thus, it is important to consider the parameters of metal gettering in Si to find the optimized thermal budget of the haze process. The gettering efficiency of OPs in Si to the metal contamination shows a threshold behavior relative to the total inner surface of defects [36,37], as follows:

$$S = 4\pi r^2 D \cdot d_{wafer} \quad (1)$$

where $r$ and $D$ are the average radius and density of precipitates, respectively, and $d_{wafer}$ is the wafer thickness. If the growth of precipitates

is sufficient, the total inner surface S is determined by the precipitate density which is affected by the amount of precipitate nucleation during the thermal process. In the vacancy-dominated region, the border that satisfies the threshold value of S moves gradually toward lower vacancy concentrations with increasing nucleation times, and the haze width formed in the lower vacancy concentration region or interstitial-dominated region becomes narrower. This condition is established when Y ≥ 180 min. However, if the precipitate growth is insufficient to reach the threshold value of S in the vacancy-dominated region, the gettering of background contaminants barely occurs and the selective nature of new haze in the point defect region does not appear. In summary, we determined that the process conditions of (X, Y) = (100, 180) min form a stable haze equivalent to the Cu haze in the shortest processing time.

If the second step time is < 120 min, haze becomes diminished or non-uniformly distributed, losing the ability to visualize the interstitial-dominant region. This suggests that temperature of the second step (1000 ˚C) is related to both the growth of OPs for the background metal gettering in the vacancy-dominated region and the formation of surface defects themselves on the interstitial-dominated region. The second step may supply Ni contaminants to the wafer surface. If the ambient metal level of the furnace is low, a long hold time in the high-temperature process is necessary to reach a metal concentration sufficient for the formation of surface defects. According to the Ni–Si binary phase diagram [38], the second-step temperature is slightly higher than the highest melting temperature (993 ˚C) of $NiSi_2$ in the dilute Ni region. Therefore, Ni adsorption and complete dissolution on a wafer are possible with the lowest consumption of Ni by the undesirable low-temperature silicide phases during the heating process.

One limitation of this method is the reliance of the contamination sources on the background level of transition metals during furnace processing; the haze uniformity is somewhat unstable under the present conditions. It is obvious that background contamination depends on the structure, materials, runtime, and cleanliness of the furnace, which are difficult to experimentally control. Further research on the process optimization that enhances the formation of surface defect is required to overcome the problems on the unspecified contamination of background haze.

## 4. Conclusion

The most important point of this study is that background haze, which has been reported only from wet oxidation processes at elevated temperatures, can be adjusted to decorate the interstitial-dominated region of CZ-Si by adding prior low-temperature oxidation steps. With the combination of 870 ˚C and 1000 ˚C precipitation steps to the 1150 ˚C wet-oxidation step, we could endow selectivity to the Ni-based background haze, which allows visualization of the point defect distribution in the Si wafer. The width of the new haze was optimized with respect to that in the regular method by adjusting the process times of the first two steps. We found that new haze widths depended significantly on the time of the 870 ˚C step, which is related to the nucleation of OPs in the vacancy-dominated region. Additionally, it was confirmed that the time of the second 1000 ˚C step should be at least 3 h for uniform haze formation. The second step was shown to closely relate to the formation of surface defects in the interstitial-dominated region of CZ-Si. In conclusion, the modification of the background haze via the proposed multi-step oxidation process is suggested as a promising candidate for analyzing defect regions in CZ-Si while avoiding high-concentration intentional contamination by transition metals.

## Declaration of Competing Interest

The authors declare that they have no known competing financial interests or personal relationships that could have appeared to influence the work reported in this paper.

## Acknowledgment

This research was supported by the R&D center, SK Siltron, The Republic of Korea. This research received no specific grants from funding agencies in the public, commercial, or not-for-profit sectors.

## References

[1] Hu SM. Precipitation of oxygen in silicon: some phenomena and a nucleation model. J Appl Phys 1983;52:3974. https://doi.org/10.1063/1.329204.
[2] Borghesi A, Pivac B, Sassella A, Stella A. Oxygen precipitation in silicon. J Appl Phys 1995;77:4169. https://doi.org/10.1063/1.359479.
[3] Tan TY, Gardner E, Tice W. Intrinsic gettering by oxide precipitate induced dislocations in Czochralski Si. Appl Phys Lett 1977;30:175. https://doi.org/10.1063/1.89340.
[4] Hölzl R, Fabry L, Range KJ. Gettering efficiencies for Cu and Ni as a function of size and density of oxygen precipitates in p/p- silicon epitaxial wafers. Appl Phys A 2001;73:137–42. https://doi.org/10.1007/s003390100846.
[5] Isomae S, Ishida H, Itoga T, Hozawa K. Intrinsic gettering of copper in silicon wafers. J Electrochem Soc 2002;149:G343–7. https://doi.org/10.1149/1.1475694.
[6] Uchiyama H, Matsumoto K, Mchedlidze T, Nisimura M, Yamabe K. N+ P junction leakage current caused by oxygen precipitation defects and its temperature dependence. J Electrochem Soc 1999;146:2322–7. https://doi.org/10.1149/1.1391934.
[7] Czerwinski A. The impact of platelet oxygen precipitates in silicon on the junction leakage current and the interstitial oxygen loss. J Phys: Condens Matter 2002;14:13135–40. https://doi.org/10.1088/0953-8984/14/48/360.
[8] Nakashima K, Watanabe Y, Yoshida T, Mitsushima Y. A method to detect oxygen precipitates in silicon wafers by highly selective reactive ion etching. J Electrochem Soc 2000;147:4294–6. https://doi.org/10.1149/1.1394056.
[9] Nakashima K, Yoshida T, Mitsushima Y. Measurements of size, morphology, and spatial distribution of oxygen precipitates in Si wafers using RIE. J Electrochem Soc 2005;152:G339–44. https://doi.org/10.1149/1.1877972.
[10] Sumino K, Yonenaga I. Oxygen Effect on Mechanical Properties. Semicond Semimet 1994;42:449–511. https://doi.org/10.1016/S0080-8784(08)60254-9.
[11] Ravi KV, Varker CJ. Oxidation-induced stacking faults in silicon. I. Nucleation phenomenon. J Appl Phys 1974;45:263. https://doi.org/10.1063/1.1662971.
[12] Kissinger G, Vanhellemont J, Lambert U, Gräf D, Dornberger E, Richter H. Influence of residual point defect supersaturation on the formation of grown-in oxide precipitate nuclei in CZ-Si. J Electrochem Soc 1998;145:L75–8. https://doi.org/10.1149/1.1838492.
[13] Falster R, Voronkov VV, Quast F. On the properties of the intrinsic point defects in silicon: a perspective from crystal growth and wafer processing. Phys Status Solidi B 2000;222:219–44. https://doi.org/10.1002/1521-3951(200011)222:1<219::AID-PSSB219>3.0.CO;2-U.
[14] Abdelbarey D, Kveder V, Schröter W, Seibt M. Platinum and gold diffusion monitor vacancy profiles induced into silicon wafers by aluminum alloying. Phys Status Solidi A 2013;210:771–6. https://doi.org/10.1002/pssa.201300020.
[15] Kot D, Kissinger G, Sattler A. Sensitivity enhanced FTIR investigation of defects introduced by RTA pre-treatment in Czochralski silicon wafers. Semicond Sci Technol 2017;32:104006https://doi.org/10.1088/1361-6641/aa865f.
[16] Kot D, Kissinger G, Dabrowski J, Sattler A. $VO_n$ complexes in RTA treated czochralski silicon wafers investigated by FTIR spectroscopy. ECS Trans 2018;86(10):95–103. https://doi.org/10.1149/08610.0095ecst.
[17] Alpern P, Bergholz W, Kakoschke R. Detection of fast diffusing metal impurities in silicon by haze test and by modulated optical reflectance: a comparison. J Electrochem Soc 1989;136:3841–8. https://doi.org/10.1149/1.2096559.
[18] Mule'Stagno L. A technique for delineating defects in silicon. Solid State Phenom 2002;82:753–8. https://doi.org/10.4028/www.scientific.net/SSP.82-84.753.
[19] Válek L, Stehlík Š, Orava J, Ďurík M, Šik J, Wágner T. Limits of the copper decoration technique for delineating of the V-I boundary. J Phys Chem Solids 2007;68:1157–60. https://doi.org/10.1016/j.jpcs.2007.01.038.
[20] S.-W. Wee, S.-W. Lee, K.-M. Bae, K.-S. Kim U.S. Patent 7,901,132 B2, March 8, 2011.
[21] Lee I-J, Paik U, Park J-G. Dependence of nickel gettering on crystalline nature in as-grown Czochralski silicon wafer. J Cryst Growth 2013;365:6–10. https://doi.org/10.1016/j.jcrysgro.2012.12.033.
[22] Istratov AA, Flink C, Hieslmair H, Heiser T, Weber ER. Influence of interstitial copper on diffusion length and lifetime of minority carriers in p-type silicon. Appl Phys Lett 1997;71:2121. https://doi.org/10.1063/1.119355.
[23] Weber ER. Transition metals in silicon. Appl Phys A 1983;30:1–22. https://doi.org/10.1007/BF00617708.
[24] Shimura F, Tsuya H, Kawamura T. Surface- and inner-microdefects in annealed silicon wafer containing oxygen. J Appl Phys 1980;51:269. https://doi.org/10.1063/1.327419.
[25] Tsuya H, Shimura F. Transient Behaviour of Intrinsic Gettering in CZ Silicon Wafers. Phys Status Solidi A 1983;79:199–206. https://doi.org/10.1002/pssa.2210790122.
[26] Shimura F, Craven RA. The Physics of VLSI. New York: AIP; 1984. p. 205.
[27] Stacy WT, Allison DF, Wu T-C. Metal decorated defects in heat-treated silicon wafers. J Electrochem Soc 1982;129:1128–33. https://doi.org/10.1149/1.2124041.
[28] Voronkov VV. Grown-in defects in silicon produced by agglomeration of vacancies and self-interstitials. J Cryst Growth 2008;310:1307–14. https://doi.org/10.1016/j.jcrysgro.2007.11.100.
[29] Jenkins MW. A new preferential etch for defects in silicon crystals. J Electrochem

Soc 1977;124:757–62. https://doi.org/10.1149/1.2133401.
[30] Hwang D-H, Hur S-M, Lee K-H. The influence of point defect on the behavior of oxygen precipitation in CZ-Si wafers. J Cryst Growth 2003;249:37–43. https://doi.org/10.1016/S0022-0248(02)02093-6.
[31] Huber W, Pagani M. The behavior of oxygen precipitates in silicon at high process temperature. J Electrochem Soc 1990;137:3210–3. https://doi.org/10.1149/1.2086188.
[32] Puzanov NI, Eidenzon AM. The effect of thermal history during crystal growth on oxygen precipitation in Czochralski-grown silicon. Semicon Sci Technol 1992;7:406–13. https://doi.org/10.1088/0268-1242/7/3/022.
[33] Graff K. Metal impurities in silicon-device fabrication. 2nd ed. Berlin: Springer; 1999.
[34] Lee AJ, Im J-S, Kang H-B, Lee S-W. Defect formation of nickel-incorporated large-diameter czochralski-grown silicon and their effect on gate oxide reliability. ECS J Solid State Sci Technol 2016;5:P3008–12. https://doi.org/10.1149/2.0021604jss.
[35] Shimura F. Semiconductor silicon crystal technology. 1st ed. CA: Academic Press; 1989.
[36] Sueoka K, Akatsuka M, Ono T, Asayama E, Koike Y, Adachi N, et al. Oxygen precipitation behavior and its optimum condition for internal gettering and mechanical strength in epitaxial and polished silicon wafers. Electrochem Soc Proc 2000;17:164–79.
[37] Hoelzl R, Blietz M, Fabrey L, Schmolke R. Gettering efficiencies and their dependence on material parameters and thermal process: How cah this be modeled? Electrochem Soc Proc 2002;2:608–25.
[38] Massalski TB, Subramanian PR, Okamoto H, Kacprzak L. Binary alloy phase diagrams. second ed. Materials Park, OH: ASM International; 1990.

**Anselmo Jaehyeong Lee** was born in Daegu metropolitan city, The Republic of Korea in 1986. He received the B.S. and M.S. degrees in materials science from the Seoul National University, Seoul in 2009 and 2011, respectively. Since 2011, he has been a senior researcher with the R&D Center, SK Siltron, Gumi city. He is the author of 4 academic articles and 16 inventions on semiconductor defect engineering and characterizations. His research interests include the behavior of grown-in and process-induced defects, gettering of metal contamination, and development of new metrology on semiconductor materials and processing.